Acceleration of foils by a pulsed laser beam

L. A. Bol'shov, I. N. Burdonskiĭ, A. L. Velikovich, V. V. Gavrilov, A. Yu. Gol'tsov, E. V. Zhuzhukalo, S. V. Zabyalets, V. P. Kiselev, N. G. Koval'skiĭ, M. A. Liberman, L. S. Mkhitar'yan, M. I. Pergament, A. I. Yudin, and A. I. Yaroslavskiĭ

I. V. Kurchatov Institute of Atomic Energy, Moscow; Institute of Physical Problems, Academy of Sciences of the USSR

(Submitted 29 July 1986)
Zh. Eksp. Teor. Fiz. **92**, 2060–2075 (June 1987)

The ablative acceleration of thin metal foils and organic films, used to simulate the shells of spherical targets for laser fusion, has been studied by a variety of approaches under strictly controlled conditions. The target was irradiated with a 3-ns pulse from a neodymium laser ($\lambda = 1.06$ mm) with a comparatively short rise time (0.3 ns) and an irradiance in the range 10^{13}–10^{14} W/cm^2. The properties of the resulting plasma corona, the mass rate of the ablation, the pressure at the ablation surface, and the properties of the accelerated part of the target were measured by various methods. The hydrodynamic acceleration efficiency was determined from the experimental data. All these results are compared with the predictions of analytic models and the results of two-dimensional hydrodynamic calculations. During stable acceleration of the plasma at the back side of the bombarded foil, which is heated to ~ 10 eV by the shock wave and the x radiation from the corona, the maximum detected velocity of the directed motion was 150 km/s, and the hydrodynamic efficiency of the acceleration was $\sim 5\%$.

1. INTRODUCTION

The conditions required for a demonstration experiment in the laser-fusion program, including estimates of the required properties of the laser light and the development of the optimum designs of spherical shell targets, depend in a fundamental way on how well we understand the physical processes and events which displayed during the irradiation of targets. It accordingly becomes important to acquire reliable data on the mechanisms for the absorption of the laser light, the properties of the plasma corona which forms, the energy transport out of the absorption zone to the ablation surface, the stability of the ablative acceleration of the piston shell which compresses the fusion fuel, and the hydrodynamic acceleration efficiencies which are attainable in devices with comparatively modest parameters. Comparison of these results with the results of analytic and numerical calculations will serve as a test of the present understanding and will ultimately improve the reliability of predictions for a planned large-scale experiment.

Extensive opportunities for experimental modeling of several processes of major importance to laser fusion have been opened up by experiments on the bombardment of thin foils and organic films by intense laser beam in slab geometry. This approach substantially simplifies the diagnostics and makes it a comparatively simple matter to distinguish the phenomena of interest from related processes for a detailed study of this phenomenon. Furthermore, less effort is required to alter the experimental conditions. On the other hand, it should be kept in mind that the validity of extrapolating the results and conclusions to spherical geometry must be evaluated in each specific case.

In this paper we report research on the acceleration of thin foils by pulses from a neodymium laser ($\lambda = 1.06$ mm) which has been carried out at the Mishen' facility at the Kurchatov Institute of Atomic Energy in Moscow. The purposes of this research were to use a variety of methods to study the ablative acceleration of targets and to compare the experimental data with simple analytic calculations and numerical simulations in order to evaluate various ideas regarding the physical processes which occur when laser light interacts with targets. The results which had been found earlier[1] at the Mishen' and also in other laboratories[2,3] provided evidence that the thermodynamic state of the accelerated matter, the maximum velocity achievable during the acceleration, the hydrodynamic efficiency achievable during the acceleration, the onset of instabilities, and the "breakup" of the dense part of the accelerated shell depend strongly on the rise time of the laser light intensity (the steepness of the leading edge of the laser pulse), the energy contrast of the pulse which bombards the target, the average diameter of the focal spot, and the distribution of the laser light intensity in this spot. These parameters were controlled in each of our experiments.

The neodymium-glass laser system of the Mishen' is described in detail in Ref. 4. Here are some typical parameters of the light emitted by the Mishen' facility under the conditions of these experiments: The energy of the laser light was $E = 200$ J; the pulse length at half-maximum was $t = 3.0$ ns; the rise time of the light intensity between the levels of 0.1 and 0.8 of the maximum intensity was $t_\Gamma = 0.3$ ns; the cross-sectional area of the beam at the exit was $S = 40 \times 240$ mm^2; the energy contrast of the laser system was $g = E_{\text{pulse}}/(E_{\text{total}} - E_{\text{pulse}}) > 10^6$; and the average divergence of the output beam was $\alpha \approx 2 \cdot 10^{-4}$ rad.

The experimental conditions were chosen in order to achieve a regime of ablative acceleration at a moderate light irradiance, $I = 10^{13}$–10^{14} W/cm^2. This regime is presently regarded as the most promising approach for the fusion ignition of a deuterium-tritium fuel in an arrangement with direct bombardment of spherical targets.

2. PARAMETERS OF THE PLASMA CORONA

The profiles of the electron density and temperature in the plasma corona at the Mishen' facility were determined experimentally by methods involving measurements of the

 0038-5646/87/061160-10$04.00

x-ray emission from the plasma with spatial, temporal, and spectral resolution. An analysis of pinhole photographs of the plasma burst taken in x radiation of different hardness levels made it possible to reconstruct time-integrated distributions of the density and the temperature. The spectrum of the continuum x-ray emission was studied by the standard method of absorbing filters. During irradiation of aluminum foils, the density and temperature profiles were also determined from measurements of the relative intensities of the spectral lines of multiply charged aluminum ions, carried out with the help of an x-ray spectrograph using a plane quartz crystal as dispersive element. A slit ~30 mm wide in front of the crystal permitted spatial resolution in the measurements in the direction perpendicular to the dispersion direction. The temperature of the plasma electrons was found from the ratio of the intensities of lines of hydrogen- and helium-like ions of aluminum; the density was determined from the ratio of the intensities of resonant and intercombinational lines of the helium-like ion, AlXII (Ref. 5). The time evolution of the x-ray emission was studied with a high-speed x-ray image converter operating in a streak-camera mode with a resolution ~20 ps and also with the help of vacuum photodiodes. The total energy of the x-ray emission was measured by photocalorimeters mounted on the wall. The procedures, apparatus, and calculation models used in this study are described in detail in Refs. 1 and 5. In several of the experiments, we used a method of "marker trajectories" in the spectroscopic measurements of the density and the temperature. In this method, layers of a material with a relatively high Z (aluminum) are deposited in small areas (~30 mm in size) on the surface of the target to be bombarded, made of a material with a relatively low Z (Lavsan, a polyester). The effect was to create a spatially periodic structure with a given period. In this case, with the appropriate choice of filters, the pinhole photographs of the plasma corona revealed "jets" emerging from the vicinity of these islands of high-Z material on the target surface. Recordings of the emission spectra of individual jets made possible local measurements of the plasma properties with a spatial resolution determined by the width of the jet. The presence of a narrow jet of "aluminum plasma" in a corona of "Lavsan plasma" eliminates the difficulties in interpretation which stem from the need to allow for reabsorption of radiation (especially for resonant lines). Figure 1 shows images of the plasma corona in the light of spectral lines of multiply charged aluminum ions. Figure 2 shows pinhole photographs of a plasma corona, taken during the bombardment

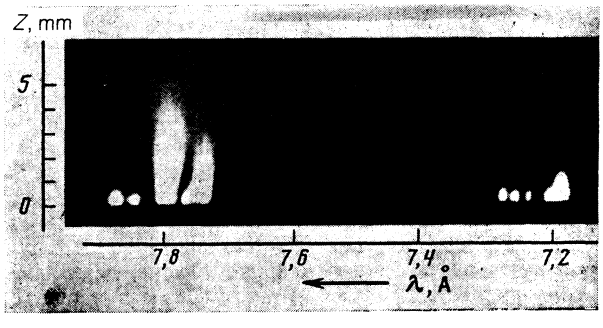

FIG. 1. Images of a plasma corona in the light of spectral lines of H- and He-like aluminum ions ($I = 5 \cdot 10^{13}$ W/cm^2).

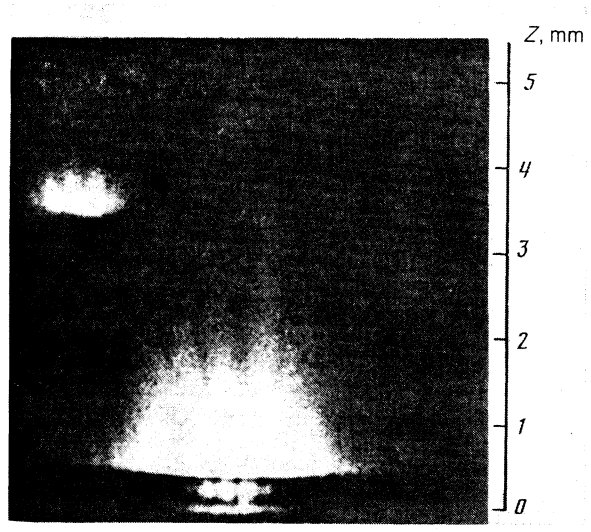

FIG. 2. Top—Pinhole photographs of a plasma corona taken during irradiation of a Lavsan target on whose surface there are aluminum "spots" bottom—behind filters of Al, 15 μm thick, and Be, 40 μm thick ($I = 5 \cdot 10^{13}$ W/cm^2).

of a Lavsan target with aluminum spots on the bombarded surface.

Figure 3 shows some typical profiles of the electron density and temperature in the plasma corona in the direction along the axis of the incident laser beam, for the case of an aluminum target, with a focus size 200 mm and a light irradiance of $5 \cdot 10^{13}$ W/cm^2. It should be noted that far from the target surface, in the low-density regions of the plasma corona, the density values found by the methods of x-ray spectroscopy agree well with the results found by interferometric measurements.[1]

To determine the rate of ablation of material from the target surface, we deposited layers of the material of interest, with a relatively low Z, with various thicknesses, on a substrate of a material with a relatively high value of Z. The x-ray emission from the plasma produced during the irradiation of two-layer targets of this sort was measured either with a crystal spectrograph or with an x-ray image converter operating in a streak-camera mode. During complete evaporation of the layer deposited on the substrate, and upon the appearance in the plasma corona of ions of the high-Z material, we detect the spectral lines of the substrate ions. The greatest thickness of the deposited layer at which these lines

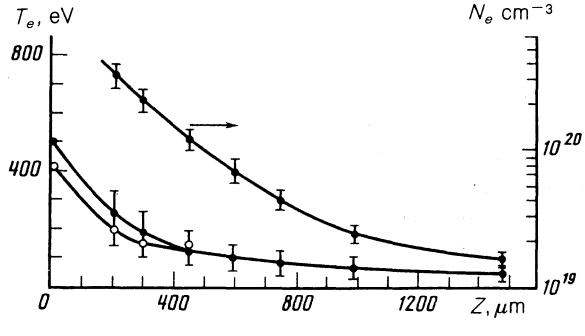

FIG. 3. Profiles of the density and temperature in the plasma corona at the axis of the incident laser beam with $I = 5 \cdot 10^{13}$ W/cm^2. ○—Measured by the method of absorbing filters; ●—measured from the slope of the photorecombination continuum of the Al×II ion.

can still be seen on the spectrogram can thus be taken to be the depth to which the ablation front penetrates into the target from the coating material during the laser pulse. This approach eliminates the need for a series of successive experiments on the irradiation of two-layer targets with different thicknesses of the layers of the material interest deposited on substrates. The ablation rate can be found in a single experiment if the thickness of the layer is chosen to be smaller than the depth to which the ablation front penetrates into the target and if the x-ray emission is measured with an x-ray image converter with good temporal resolution. From the densitometer trace of the signal from the screen of the x-ray image converter shown in Fig. 4 we can find the rate of evaporation of a surface layer of aluminum of given thickness deposited on a copper substrate (1.5 μm in 1.5 ns).

Table I lists the basic parameters of the plasma corona for the case of an aluminum target under typical irradiation conditions in Mishen', for a laser-beam irradiance of $5 \cdot 10^{13}$ W/cm^2. Also shown here are estimates of the abiation pressure, the ablation rate, and the characteristics of the x-ray emission and the superthermal electron component found in numerical calculations carried out with the Impul's code, developed for the purpose.[6] The one-dimensional and two-dimensional MHD programs of the Impul's code systematically incorporate the absorption of the laser light, the electron thermal conductivity, the ionization kinetics, the energy exchange between electrons and ions, and the intrinsic bremsstrahlung and recombination emission from the plasma, with allowance for self-absorption. A realistic equation of state[7] was used to describe the dense inner regions of the target.

From the parameter values shown in Table I we can draw some conclusions.

Under these conditions, we are dealing with an "extended" plasma corona, with length scales for the gradients of the density and the temperature in the regions with densities $n \leqslant n_{cr}$ which are 100–200 times as long as the wavelength of the laser light. The primary absorption mechanism is classical collisional absorption. The number and energy of the superthermal electrons produced as a result of parametric instabilities are relatively small. (The measured values of the absorption coefficient for the laser light, with the wavelength 1.06 μm, range up to 80–90%.)

The difference between the measured and calculated coefficients of the conversion of laser energy into cw x-ray emission (columns 2 and 3 in Table I) arises because the measurements were carried out at x-ray energies above 0.8 keV; these x rays are emitted primarily from regions of the plasma corona with the highest temperature, near the absorption zone. The results of the measurements were then extrapolated to x-ray energies between 0.1 and 0.8 keV. Consequently, these results ignore that component of the total energy of the x-ray emission which is represented by x rays with comparatively low energies, which are emitted from regions of dense plasma, with a relatively low temperature, between the ablation surface and the critical-density surface.

During irradiation of aluminum targets, the fraction of the laser light energy converted into the line emission of multiply charged ions was found to be several times higher than that for conversion into the x-ray continuum emitted by the plasma. It should be noted, however, that line emission is a comparatively small component of the heating of the (unevaporated) part of the foil which is being accelerated. Measurements showed[5] that the region of the emission of the line spectrum during irradiating of aluminum targets stretches out 3 or 4 mm from the surface, and the emission time of the multiply charged ions is substantially longer than the laser pulse.

Under these conditions, an ablation acceleration regime prevails during the irradiation of aluminum foils a few microns thick. There is no intense preheating by superthermal electrons of the material being accelerated. Numerical cal-

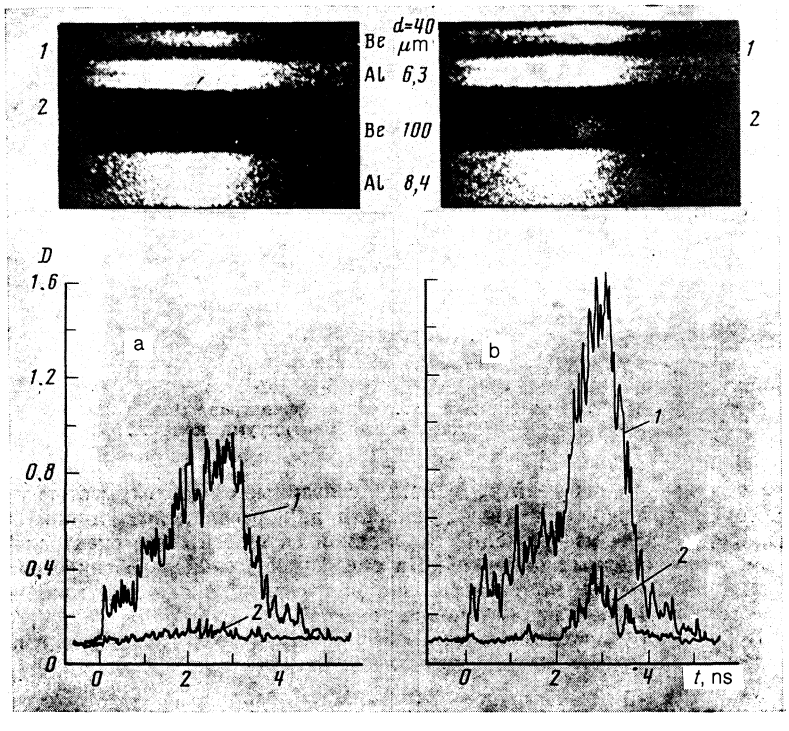

FIG. 4. Densitometer traces of a streak image on the screen of the x-ray image converter. a—Aluminum target 6 μm thick; b—irradiation of a copper target on whose surface there is an aluminum layer 1.5 μm thick ($I = 5 \cdot 10^{13}$ W/cm^2).

TABLE I.

Property of plasma corona	Numerical calculation	Experiment
ΔS, cm^2	...	$(0.5-1)\cdot 10^{-3}$
Δl, μm	90 – 120	50 – 100
$L = n/\nabla n$, μm	100	100
T_e, keV	0.7 – 0.8	0.5
c_s, cm/s	$(1.8-2)\cdot 10^7$	$1.5\cdot 10^7$
λ_{ei}, μm	1.5	1.0
K_{cont}, %	2 – 2.5	1 – 1.5
K_{line}, %	...	4 – 5
T_{st}, keV	...	3–5
$W_{\text{st}}/W_{\text{therm}}$	...	$10^{-4}-10^{-3}$
dm/dt, g/ns	$(0.8-1.2)\cdot 10^{-7}$	10^{-7}
P_a, Mbar	4 – 5	2 – 3

Note ΔS—Typical size of the irradiated surface; Δl—distance from the ablation surface to the critical-density surface; $L = n/\nabla n$—length scale of the variations in the density near the critical-density surface; T_e—electron temperature in the region with the critical density; c_s—sound velocity at the critical surface (for an effective ion charge $Z = 11$); λ_{ei}—electron mean free path ($\lambda_{ei} = 3\cdot 10^{12} T_e\,[\text{eV}]/Zn_{\text{cr}}$); K_{cont}—coefficient of the conversion of laser energy into continuum emission from the plasma corona with a photon energy > 0.1 keV; K_{line}—coefficient of the conversion of laser energy into line emission of multiply charged aluminum ions; T_{st}—temperature of the superthermal electrons; $W_{\text{st}}/W_{\text{therm}}$—relative energy of the superthermal electron component; dm/dt—ablation rate; P_a—ablation pressure.

culations[8] showed that for the parameter values for the superthermal electrons which are listed in Table I the temperature of the accelerated matter is raised by the heating caused by these electrons is no more than 0.5 eV in the case of an aluminum foil with a thickness of 5–10 mm. We find substantially higher temperatures (but less than 5–10 eV) when we consider the heating of the accelerated material by the shock wave and by the "soft" x-ray emission from the plasma corona. The time taken by the shock wave to propagate through the unevaporated part of the target is about 0.5 ns (since the velocity of the shock front in Al at a pressure of 2–3 Mbar behind the front is about 10^6 cm/s). In other words, this transit time is several times shorter than the laser pulse, and the directed velocity acquired during the operation of the ablation piston is substantially higher than the thermal velocity of the particles of the material being accelerated.

Figure 5, a–c, shows interferograms of the plasma corona found by sending light beams tapped from the main beam through the region where the laser beam interacts with an aluminum foil with dimensions of 6×15 mm^2 and a thickness of 6 mm. (After conversion to the second harmonic, with $\lambda = 0.53$ mm and shortening of the pulse to 0.3 ns, the probing beams, which propagate at small angles with respect to each other, pass through the plasma under study with a time delay.) We see that by the end of the laser pulse (the second frame) the transverse dimensions of the region in which the plasma is produced at the irradiated surface are substantially greater than the size of the focal spot. Later on, a dense plasma slab is produced in the form of a conical shell in the peripheral regions of the plasma corona. This slab expands away from the surface of the target (sharp jogs of the interference fringes are observed along the generatrices of a truncated cone; the angle at which these generatrices are inclined with respect to the irradiated surface increases with decreasing Z of the target material). As can be seen from the interferograms in Fig. 5, effective acceleration of material at the back side of the foil occurs only within an area with dimensions close to the size of the focal spot. The ablation rate and the temperature of the plasma produced in the peripheral regions at the surface of the foil on the irradiated side are thus comparatively low. It may be that the production of plasma in the peripheral regions of the target, with transverse dimensions far greater than the dimensions of the focal

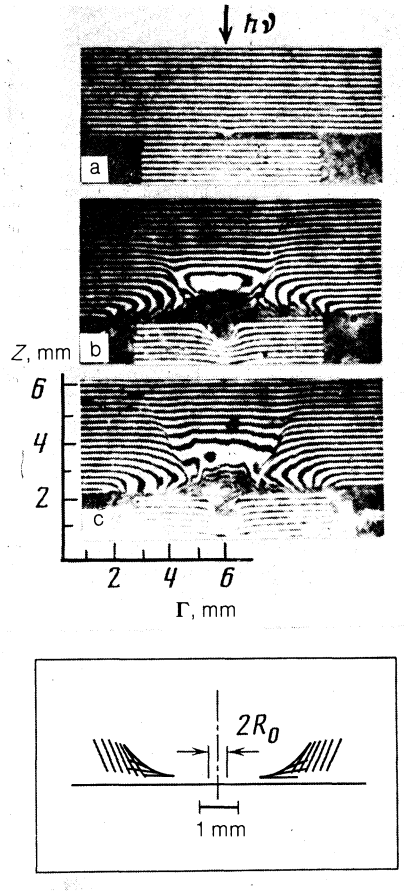

FIG. 5. Interferograms recorded at successive times during the irradiation of an aluminum foil 6 μm thick at $I = 5\cdot 10^{13}$ W/cm^2. a—2 ns; b—4 ns; c—10 ns. Shown at the bottom are the directions corresponding to the solutions of Eq. (1) for the successive times. The envelope shows the region in which the plasma stream deflects away from the focal spot toward the normal to the target surface.

spot, occurs when the laser light acts on the surface (the "wings" of the intensity distribution in the beam cross section or rays refracted by the plasma) and as the soft x radiation from the plasma corona acts on the surface. The observed conical structure then arises because the hot plasma expanding from a region with dimensions on the order of the diameter of the focal spot interacts with the nearly planar flow of low-temperature plasma propagating along the normal to the surface of the foil over areas substantially greater than the area of the focal spot.[1]

These arguments are supported by calculations based on the use of simple self-similar solutions to describe the plasma streams. The hydrodynamic flow in the direction along the target surface which is caused by the thermal expansion of the hot plasma is deflected by the planar flow of low-temperature plasma which is propagating along the normal to the surface. This deflection occurs at points determined by equating the momentum fluxes carried by the two flows. The corresponding local deflection angle can be found from the equation

$$p_0+\rho_0 v_0^2 \sin\varphi = p_1+\rho_1 v_1^2 \cos\varphi, \qquad (1)$$

where p, r, and v are the pressure, density, and velocity of the plasma at the point under consideration, and the subscripts 0 and 1 specify the expanding corona and the plane flow of low-temperature plasma, respectively. During adiabatic expansion of a hot plasma corona, the pressure p_0 falls off rapidly with increasing outer radius ($p_0 \sim R^{-5}$). Beginning at some value of R for which the condition $p_0 = \rho_1 v_1^2$ holds, Eq. (1) has solutions. Figure 5d shows line segments whose inclination with respect to the target surfaces is determined by the solution of (1) for the case in which the distribution of the laser light intensity at the target is approximated by two Gaussian distributions: one (the main one) with a half-width of 200 μm, and the other with a half-width of 2 mm and a total energy amounting to $\sim$0.5% of the energy of the main incident pulse.

Special experiments revealed the relative importance of the various factors in the evaporation (ablation) of material from the zones on the target surface which are peripheral to the focal spot. In these experiments, we irradiated Lavsan films with an area of 6×6 mm^2 and a thickness of 10 μm, on whose back surface a layer of aluminum with a thickness of order 0.1 μm had been deposited. Shadow photographs demonstrating the motion of the aluminum at the back surface of the target for the case in which an opaque screen with a slit passing most of the laser beam was positioned above the irradiated film, at a distance of 1 mm from it, were compared with corresponding photographs obtained without this screen. The fact that the acceleration of the material within the focal spot is indentical in the two cases is evidence that the ablation pressure at the target surface near the axis of the laser beam is essentially identical. The screen does not alter the characteristics of the plasma corona; the intensity and spectrum of the x-ray emission from the plasma remain the same, as do the density gradients, which determine the refraction of the laser light incident on the target. Without a screen to limit the beam, evaporation of the aluminum layer is observed over essentially the entire back surface of the Lavsan film. When the screen is in place, aluminum is evaporated only within the area of the focal spot. This result is evidence that the main reason for the evaporation of material and the production of a comparatively cool plasma in the peripheral parts of the target surface in our experiments is the presence of broad "wings" on the distribution of the light intensity over the cross section of the laser beam. In contrast with a Lavsan film, an aluminum foil, used as the target in most of the experiments, is a fairly effective screen for the laser light from the very beginning of the laser pulse, and no evaporation of material occurs in the peripheral regions on the back surface of the aluminum foils.

In several of the experiments, jet structures are observed on the pinhole photographs of the plasma corona (Fig. 6), and on the shadow photographs one can see a multitude of filamentary formations near the surface of the foil. These filamentary formations are scattered in a disordered way in regions several times the size of the focal spot (see Fig. 9 below). Jet structures have been distinguished, and mechanisms which might be responsible for their formation have been analyzed, in Ref. 7. An experimental study of these events goes beyond the scope of the present study. Here we simply wish to state the fact that over the broad ranges of conditions which we studied the properties of the acceler-

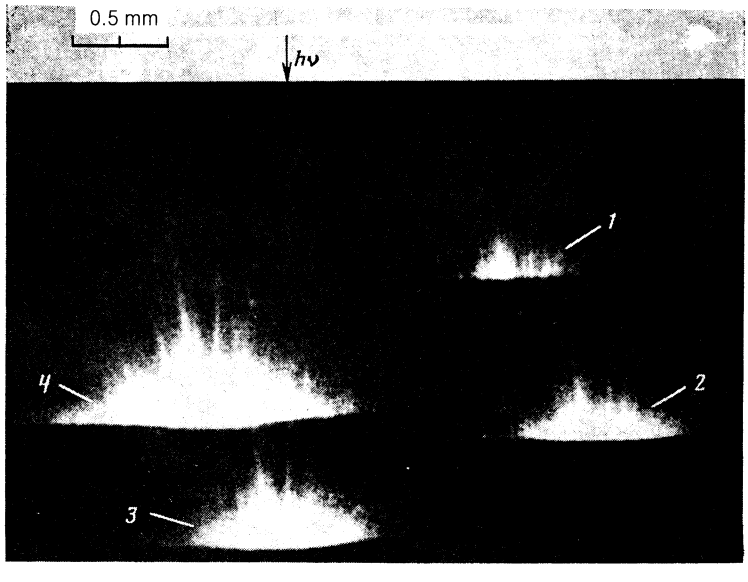

FIG. 6. X-ray pinhole photographs of the plasma corona recorded with various filters. 1—Aluminum, 18 μm thick; 2—aluminum 14.7 μm thick; 3—aluminum, 12.4 μm thick; 4—beryllium, 40 μm thick (Lavsan target 10 μm thick at $I = 5\cdot 10^{13}$).

ated foil material and the basic features of the acceleration process remain essentially independent of the presence or absence of such structures.

3. STUDY OF THE ACCELERATED UNEVAPORATED PART OF THE FOIL

3.1. Properties of the accelerated part of the foil

Let us consider certain features of a qualitative nature which are observed on the interferograms and shadow photographs taken at successive times in experiments on the irradiation of thin foils. Figure 7 shows some pertinent interferograms, which correspond to various times up to 13 ns after the beginning of the laser pulse. An aluminum foil 6 μm thick was irradiated in a nitrogen atmosphere ($p = 5$ Torr) at an intensity of $5 \cdot 10^{13}$ W/cm^2. The transverse dimensions of the opaque zone observed on the back side of the foil are seen to be essentially the same as the dimensions of the focal spot. The boundary of the opaque zone in the direction perpendicular to the surface gradually slows down, and after 15–20 ns we observe an essentially complete halt of the shadow boundary, at a distance of order 400 mm from the foil. As the boundary of the opaque zone moves away from the target, the transverse dimensions of the shadow region increase slightly. The bending of the interference fringes near the rather substantially blurred boundary of the opaque zone on the back side of the target is evidence of ionization of the material being accelerated. We can clearly see the fronts of shock waves excited in the gas around the target, on both the irradiated side and the back side of the foil.

Because of the pronounced refraction of the probing light and the difficulties in using high-speed converging optics in the five-frame interference arrangement which we used, the position of the shadow boundary corresponds to plasma densities more than an order of magnitude below the critical density for the wavelength $\tau = 0.53$ mm ($n_e \sim 10^{20}$ cm^{-3}). Analysis of the experimental data on the expansion of the accelerated part of the aluminum foil and of time-integrated plasma emission spectra in the visible region leads to temperature values of 5–10 eV (Ref. 1). The same values were found under similar conditions by Gold and McLean.[10]

To determine the directed velocity (the velocity of the center of mass of the accelerated plasma) acquired during acceleration, we plotted the displacement velocity of the boundaries of the opaque zone seen on the shadow photographs versus the time and then determined by extrapolation the velocity at the end of the laser pulse.[1] Within the measurement error, the velocities found in this manner are inversely proportional to the thickness of the foil for thicknesses of the irradiated aluminum foils and organic films in the range 3–10 mm. For an aluminum foil with a thickness of 6 mm, and at a light irradiance of $5 \cdot 10^{13}$ W/cm^2, the velocity of the directed motion is $9 \cdot 10^6$ cm/s.

Another, independent method for determining the velocity of the material on the back side of the target, the "double-foil method," proved extremely effective. The optical diagram in Fig. 8a explains the basic features of this method. A camera with a fast image converter operating in a streak-camera mode also records the light in the visible range on the back side of the foil on an auxiliary film 200–300 mm behind the irradiated foil. By choosing the thickness of this auxiliary film, its distance from the foil, and the sensitivity of the image converter appropriately in some special control experiments, we achieved conditions such that the light appeared on the auxiliary film at the same time moderately dense ($n \gtrsim 10^{21}$ cm^{-3}) layers of the accelerated plasma arrived there. Figure 8b shows a streak photograph of the light at the back side of an aluminum foil 6 mm thick and at the surface of an auxiliary foil. The reference marker in the upper left corner corresponds to the illumination of the film by the laser pulse. The beginning of the emission at the back side of the foil corresponds to the time at which a shock wave arrives there. The velocity values found from the measured time intervals between when light appeared at the back side of the foil and when the light appeared at the surface of the

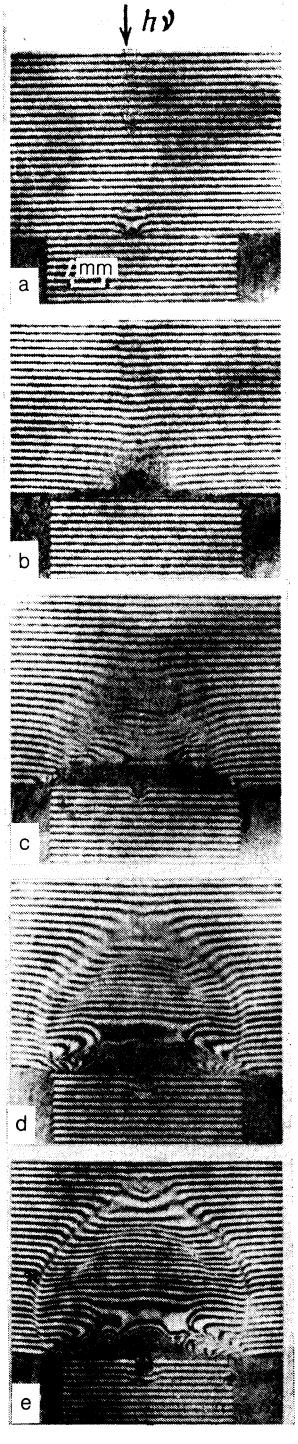

FIG. 7. Interferograms recorded at successive times during acceleration of an aluminum foil 6 μm thick in a nitrogen atmosphere (the nitrogen pressure in the chamber was 5 Torr, and the irradiance was $I = 5 \cdot 10^{13}$ W/cm^2). a—1 ns; b—4; c—7; d—10; e—13 ns.

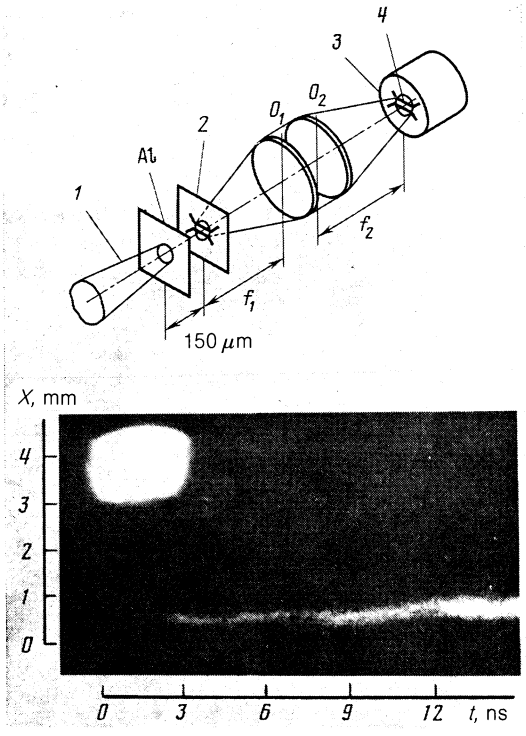

FIG. 8. a: Optical arrangement used to determine the velocity of the material of the back side of the target by the double-foil method. 1—Laser; 2—Lavsan; 3—image converter; 4—slit. b: Streak photograph of the emission at the back side of an aluminum foil 6 mm thick and at the surface of an auxiliary Lavsan film. The spot at the top is the light pulse.

auxiliary film, for a given distance between the foil and the film, agree well with the results of measurements of the displacement velocity of the boundary of the opaque zone on the shadow photographs. We used the double-foil method in our experiments to record the spatial distribution of the velocities in the direction perpendicular to the direction of the accelerated plasma, as in the experiments of Obenschain *et al.*[11] With a high-quality optical system to construct a magnified image of the surface of the auxiliary film in the plane of the slit of the image converter, the spatial resolution was better than 10 mm. The presence of spatial modulations of the velocity in the direction perpendicular to the direction of motion was identified with the onset of a Rayleigh-Taylor instability in the stage of the acceleration of the unevaporated part of the foil. Comparison of the data obtained by the technique described above with the shadow photographs of the plasma on the back side of the foil at later times, after the end of the laser pulse (Fig. 9), revealed the spatial wavelength of the most dangerous perturbation mode. According to these measurements, which were carried out under conditions such that the distribution of the irradiance of the laser beam over the focal spot varied by less than 10–20% (these variations were controlled in each experiment), the spatial wavelength of the best-expressed instability mode was five or six times the thickness of the accelerated foil. There is no correlation of any sort between the spatial distribution of the velocities on the back side of the target and the patterns of

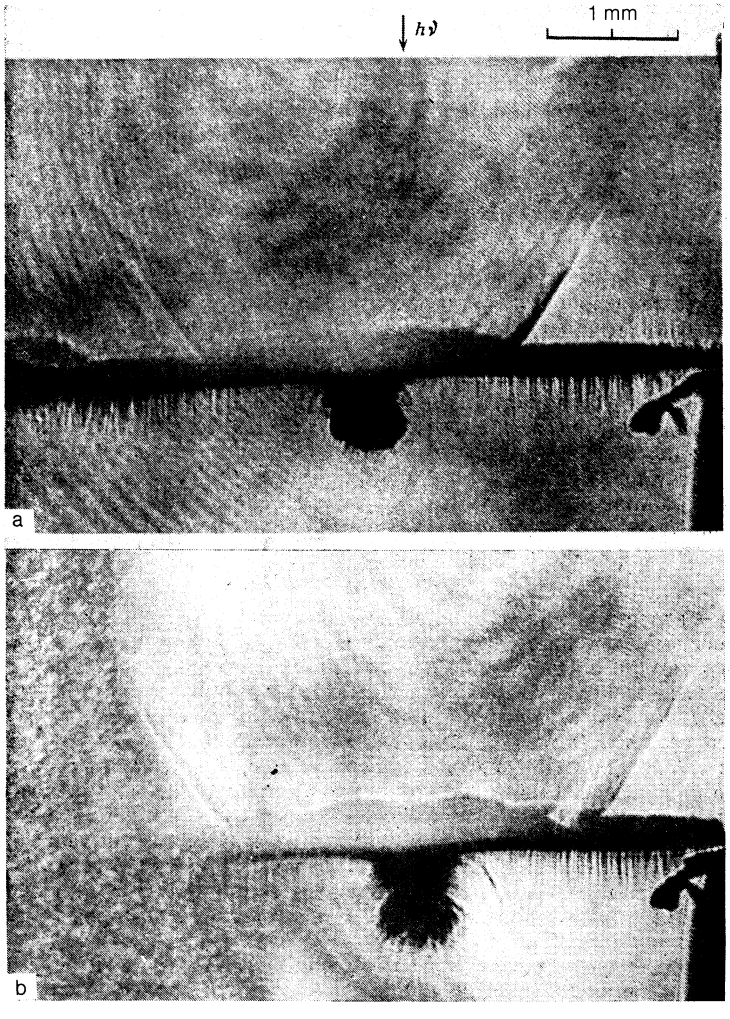

FIG. 9. Shadow photographs demonstrating the onset of an instability during the acceleration of Lavsan film 5 μm thick ($I = 5 \cdot 10^{13}$ W/cm^2). a—5 ns; b—9 ns.

the distribution of the irradiance within the focal spot which were observed in these experiments.

To determine the velocity of the directed motion of the target, we supplemented the methods described above with a new method based on measurements of the velocity of the front of the shock wave excited during motion of the accelerated part of the foil through the low-density gas[12] ($p = 2$–5 Torr). The velocity of the "piston" found from the observed velocity of the shock wave agrees well with the values found by other methods.

3.2. Determination of the foil velocity from the velocity of the boundary of the opaque zone

The accelerated unevaporated part of the foil is a plasma whose expansion occurs against the background of its motion as a whole at a constant velocity along the direction of the incident beam. The shadow photographs and interferograms show records of successive positions of the surface with a given value $n_e \sim 4\cdot 10^{20}$ cm^{-3}. The velocity of this surface is a phase velocity, since its motion is not directly related to the motion of the plasma particles. The slowing and stopping of the boundary of the opaque zone on successive shadow photographs can be explained in the following way. The phase velocity of the boundary of the opaque zone can be found by differentiating the relation $n_e(z - ut, t) = n_1 = \text{const}$. Doing this, we find the following expression:

$$\left(\frac{dz}{dt}\right)_{n_e=n_1} = u - \frac{(\partial n_e/\partial t)_{n_e=n_1}}{(\partial n_e/\partial \xi)_{n_e=n_1}}, \qquad (2)$$

where z is the coordinate along the axis of the laser beam, and $\xi = z - ut$. If the plasma density profile at the beam axis is bell-shaped, the condition $\partial n_e/\partial \xi < 0$ will hold at its leading edge. Accordingly, when the density profile begins to spread, and the surface of a constant density $n_e = n_1$ moves forward away from the center of mass of the plasma as a result of thermal expansion, we have $(\partial n_e/dt)_{n_e=n_1} > 0$; i.e., the observed velocity of the shadow boundary, dz/dt, is greater than the velocity of the center of mass, u. Later on, when n_1 approaches the maximum value which characterizes the profile at the given instant, the derivative $(\partial n_e/dt)_{n_e=n_1}$ changes sign, going negative, while $(\partial n_e/\partial \xi)_{n_e=n_1}$ decreases in absolute value, approaching zero. As a result, the velocity of the shadow boundary gradually decreases, and just before the maximum density falls below n_1 the boundary of the opaque zone comes to a halt, as can be seen on the shadow photographs.

The experimental results on the expansion of the plasma after the end of the laser pulse can be interpreted with the help of (2) and the known[13,14] self-similar solutions of the problem of the expansion of a gas ellipsoid into vacuum. Approximating the accelerated part of the target as an axisymmetric plasma ellipsoid which initially is highly oblate along the direction of motion and which has semiaxes equal to, respectively, the radius of the focal spot, R_r and half the initial thickness of the unevaporated part of the target, d_r, we find $z - t$ and $r - z$ diagrams for the motion of the shadow boundary (Fig. 10).

Analysis of the self-similar solutions shows that the thermal expansion of the accelerated part of the foil occurs primarily along the axis of the laser beam (along the direction of the greatest pressure gradient). Using the explicit

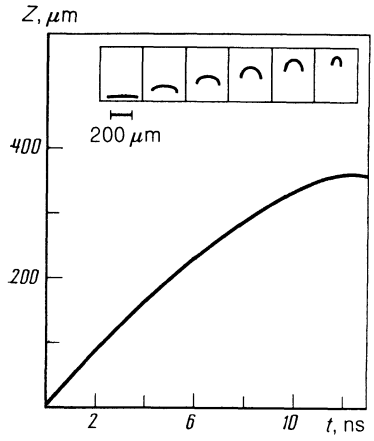

FIG. 10. z-t diagram of the motion of the shadow boundary (the density level is $n_e = 4\cdot 10^{20}$ cm^{-3}) along the axis of the laser beam (self-similar solution; $I = 2\cdot 10^{13}$ W/cm^2; the temperature of the accelerated part of the foil is 5 eV). The inset shows successive positions (at intervals of 2.4 ns) of the front part of the shadow boundary in the (r,z) plane.

self-similar solutions, we find the following estimate of the time at which the boundary of the opaque zone comes to a halt:

$$\tau_{\text{stop}} = \frac{d_r}{2\sqrt{3\pi}} \frac{n_0}{n_1} \left(\frac{T_0}{m_i}\right)^{-1/2}, \qquad (3)$$

when n_0 is the initial electron density, and T_0 is the initial temperature of the unevaporated part of the target. For an aluminum target with $d_r = 4$ mm, $T_0 = 5$–10 eV, and $n_0/n_1 = 100$, we find $\tau_{\text{stop}} = 11$–15 ns, in good agreement with the experimental data.

3.3. Results of numerical calculations for the accelerated part of the target

Figure 11 shows the results of one-dimensional numerical calculations of the temperature of the back side of an aluminum foil 6 mm thick under the conditions corresponding to the interferograms in Fig. 7. We see that for the given target thickness and for an absorbed irradiance $2\cdot 10^{13}$ W/cm^2 the temperature is determined by two factors: the heating of the unevaporated part of the target by the shock wave

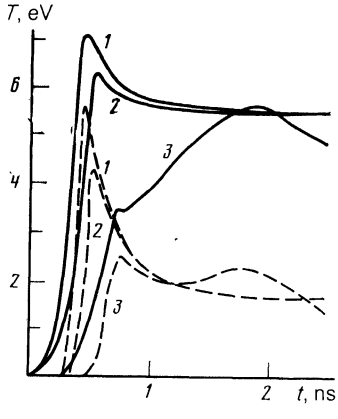

FIG. 11. Time evolution of the temperature at the back side of an aluminum foil 6 μm thick ($I = 2\cdot 10^{13}$ W/cm^2, $\tau = 3$ ns). (Solid lines). Results of calculations incorporating the heating caused by the x radiation (dashed lines); results of calculations ignoring this heating. 1—$\tau_r = 0.3$ ns; 2—0.5 ns; 3—1.5 ns.

TABLE II.

d_0, μm	u, km/s		T, eV		η, %	
	Experiment	Numerical calculation	Experiment	Numerical calculation	Experiment	Numerical calculation
3	150	160	–	12	6	8.8
6	70–80	80	~8	8.8	4	4.7
10	40–50	55	–	6	2	2.5

Note. d_0—Initial thickness of the aluminum foil; u—directed-motion velocity acquired; T—temperature of the accelerated part of the foil; η—hydrodynamic acceleration efficiency ($I = 5 \cdot 10^{13}$ W/cm^2, $\tau = 3$ ns, $\tau_\Gamma = 0.3$ ns).

propagating through it and the heating due to the absorption of x radiation emitted from the plasma corona. The amplitude of the shock wave (and therefore the temperature peak during the first 0.3–0.8 ns) depends strongly on the rise time of the laser pulse. After the shock wave emerges at the back surface of the film, a rarefaction wave propagates through the target, and the temperature at the back side decreases. The heating of the accelerated part of the foil caused by the x radiation is particularly noticeable when we make a comparison with the results of calculations ignoring the x radiation. Furthermore, an aluminum layer 2.5 μm thick "burns up" and turns into plasma in these calculations; the directed velocity of the unevaporated part is determined primarily by the ablation pressure (calibration calculations showed that the x-ray heating affects the temperature but not the velocity of the directed motion of the accelerated material).

The two-dimensional distributions, of the density calculated for various times during the laser irradiation of an aluminum foil demonstrate that the velocity of the front boundary of the shadow progressively decreases, and the actual "bleaching" is preceded by an abrupt stopping of the shadow boundary. In a series of calculations, the target thickness, the energy of the laser pulse, the length of this pulse, and the length scale of the focal spot were all varied over wide ranges. The results of a two-dimensional calculation on the motion of the shadow boundary agree with the analytic results shown in Fig. 10.

4. CONCLUSION

The results of this study can be used to optimize the conditions for the ablative acceleration of thin foils simulating the shells of fusion targets. An important characteristic of the conversion of the energy of the laser light into kinetic energy of the target is the hydrodynamic acceleration efficiency η, defined as the ratio of the kinetic energy of the accelerated part of the target to the energy absorbed from the laser pulse. Under the assumption that the velocity at which the material flows away from the surface of the irradiated foil remains constant (the velocity component along the normal to the surface is v), we can calculate the velocity acquired by the unevaporated part of the foil and also the hydrodynamic efficiency from the rocket equations

$$u = v \ln(1/x), \quad \eta = x \ln^2 x/(1-x), \tag{4}$$

where $x = 1 - j\tau/\rho_0 d_0$. According to (4), the maximum efficiency $\eta = 64.8\%$, is reached at $x = 0.2$.

When we allow for the energy expended on heating the plasma in the one-dimensional quasisteady model of the plasma corona[15] (the ablation pressure is described by $P \sim I_{\text{abs}}^{2/3}$, and the mass flux density by $j \sim I_{\text{abs}}^{1/3}$), we can replace (4) by

$$\eta = \frac{P^2}{2jI_{\text{abs}}} \frac{x \ln^2 x}{1-x}. \tag{5}$$

In particular, assuming that the Chapman-Jouguet point lies near the critical-density point in the corona, we find $P^2/2jI_{\text{abs}} = 0.1$ and $\eta_{\max} = 6.5\%$ at $x = 0.2$—in good agreement with experiment.

Experimental values of the hydrodynamic efficiency were calculated from the measurements of the energy absorbed from the laser pulse, E_{abs}, the ablation rate $dm/dt = j\Delta S$, and the velocity of the directed motion of the foil, u:

$$\eta = \frac{m(\tau)u^2}{2E_{\text{abs}}} = \frac{(\rho_0 d_0 - j\tau)u^2}{2I_{\text{abs}}\tau}, \tag{6}$$

where $m(\tau)$ is the mass of the accelerated unevaporated part of the target, and τ is the length of the laser light pulse.

Table II shows typical values of the velocity and temperature of the unevaporated parts of aluminum foils with various initial thicknesses, along with values of the hydrodynamic acceleration efficiency. Also shown here are values found for these quantities from the calculations with the Impul's code. It was concluded from the numerical calculations that the hydrodynamic efficiency increases with decreasing rise time of the laser pulse under otherwise equal bombardment conditions.

The results of this study show that the optimum thickness of the irradiated aluminum foil is 5–6 μm in the ablative acceleration of thin foils by laser pulses with a short rise time, ~0.3 ns, for laser-light irradiances in the range 10^{13}–10^{14} W/cm^2. In this case the accelerated part of the foil (roughly 50% of the foil) propagates in a stable manner over a distance up to 400–500 μm in the form of a dense plasmoid. The velocity of this plasmoid reaches 100–150 km/s, and the hydrodynamic efficiency 4–5%. During the acceleration of thin spherical shells under these conditions, one could expect the hydrodynamic efficiency to increase to ~10% because there would be no energy loss associated with the transverse expansion of a corona.

[1]Yu. A. Bondarenko *et al.*, Zh. Eksp. Teor. Fiz. **81**, 170 (1981) [Sov. Phys. JETP **54**, 85 (1981).
[2]B. H. Ripin, P. R. Whitlock, F. C. Young *et al.*, Phys. Rev. Lett. **43**, 350 (1979).
[3]W. C. Mead, E. M. Campbell, and K. G. Estabrook, Phys. Rev. Lett. **47**, 1289 (1981).
[4]V. V. Alexandrov *et al.*, Nucl. Fusion Suppl. **15**, 113 (1975).
[5]V. A. Boĭko, V. V. Gavrilov, M. I. Pergament *et al.*, Pis'ma Zh. Tekh. Fiz. **8**, 1112 (1982) [Sov. Tech. Phys. Lett. **8**, 478 (1982)].

[6]L. A. Bol'shov *et al.*, Preprint IAE-4185, I. V. Kurchatov Institute of Atomic Energy, Moscow, 1985.
[7]A. V. Bushman, A. L. Hu, and V. E. Fortov, Uravnenie sostoyaniya v éksperimental'nykh usloviyakh (Equations of State Under Experimental Conditions), Izd. ITPM SO Akad. Nauk SSSR, Novosibirsk, 1981, p. 4.
[8]R. M. More, Laser Interaction and Related Plasma Phenomena. Vol. 5. Proceedings of the Fifth Workshop (Rochester, New York), November 5–9, 1979, New York, 1981.
[9]I. Limpoukh and V. B. Rozanov, Kvant. Elektron. (Moscow) **11**, 1416 (1984) [Sov. J. Quantum Electron. **14**, 955 (1984)].
[10]S. H. Gold and E. A. McLean, J. Appl. Phys. **53(1)**, 784 (1982).
[11]S. P. Obenschain *et al.*, Phys. Rev. Lett. **46**, 1402 (1981).
[12]I. H. Burkonskiĭ, A. L. Velikovich, M. A. Liberman *et al.*, Tezisy dokl. na IV Vsesoyuzn. soveshch. po diagnostike vysokotemperaturnoĭ plazmy, Alushta, 1986 (Proceedings of the Fourth All-Union Conference on the Diagnostics of Hot Plasmas, Alushta (1986), FTI UAN, Khar'kov, 1986, p. 109.
[13]L. V. Ovsyannikov, Dokl. Akad. Nauk SSSR **111**, 47 (1957).
[14]I. V. Nemchinov, Prikl. Mat. Mekh. **29**, 134 (1965).
[15]N. G. Basov, Yu. A. Zakharenkov, A. A. Runasov *et al.*, in: Scientific and Technological Progress. Series on Radio Engineering, Vol. 26 (ed. N. G. Basov), Izk. VINITI, Moscow, 1982, Part 2.

Translated by Dave Parsons